

# **Novel methodology for the quantitative assay of fissile materials using temporal and spectral $\beta$ -delayed $\gamma$ -ray signatures**

D.H. Chivers<sup>a</sup>, K. Alfonso<sup>a</sup>, B.L. Goldblum<sup>a,b</sup>, B.A.  
Ludewigt<sup>c</sup>

<sup>a</sup>Department of Nuclear Engineering, University of California,  
Berkeley, CA 94720, USA

<sup>b</sup>Department of Nuclear Engineering, University of Tennessee,  
Knoxville, TN 37996, USA

<sup>c</sup>Lawrence Berkeley National Laboratory, Berkeley, CA 94720,  
USA

*December 15, 2010*

## DISCLAIMER

This document was prepared as an account of work sponsored by the United States Government. While this document is believed to contain correct information, neither the United States Government nor any agency thereof, nor The Regents of the University of California, nor any of their employees, makes any warranty, express or implied, or assumes any legal responsibility for the accuracy, completeness, or usefulness of any information, apparatus, product, or process disclosed, or represents that its use would not infringe privately owned rights. Reference herein to any specific commercial product, process, or service by its trade name, trademark, manufacturer, or otherwise, does not necessarily constitute or imply its endorsement, recommendation, or favoring by the United States Government or any agency thereof, or The Regents of the University of California. The views and opinions of authors expressed herein do not necessarily state or reflect those of the United States Government or any agency thereof or The Regents of the University of California.

# Novel methodology for the quantitative assay of fissile materials using temporal and spectral $\beta$ -delayed $\gamma$ -ray signatures

D. H. Chivers<sup>a</sup>, K. Alfonso<sup>a</sup>, B. L. Goldblum<sup>a,b,\*</sup>, B. Ludewigt<sup>c</sup>

<sup>a</sup>*Department of Nuclear Engineering, University of California, Berkeley, California 94720, USA*

<sup>b</sup>*Department of Nuclear Engineering, University of Tennessee, Knoxville, Tennessee 37996, USA*

<sup>c</sup>*Lawrence Berkeley National Laboratory, Berkeley, California, 94720, USA*

---

## Abstract

An analytical model for the generation of  $\beta$ -delayed  $\gamma$ -ray spectra following thermal-neutron-induced fission of mixed samples of  $^{235}\text{U}$  and  $^{239}\text{Pu}$  is presented. Using an energy-dependent figure-of-merit to designate the spectral regions employed in the assay, the unique temporal  $\beta$ -delayed  $\gamma$ -ray signatures are utilized to determine the fraction of  $^{239}\text{Pu}$  in a mixed U-Pu sample. By evaluating the  $\beta$ -delayed  $\gamma$ -ray temporal signatures of both  $^{235}\text{U}$  and  $^{239}\text{Pu}$  within a 3 keV energy bin, traditional sources of systematic uncertainty in quantitative assay using  $\beta$ -delayed  $\gamma$ -ray signals, such as self-attenuation of the sample and energy-dependent  $\gamma$ -ray detection efficiency, are significantly reduced. The effects of the time-dependent Compton-continuum and growth of longer-lived nuclides on the quantitative assessment are explored. This methodology represents a promising extension of the conventional means of analysis for quantitative assay of fissile materials using  $\beta$ -delayed  $\gamma$ -ray signatures.

*Keywords:*

Delayed  $\gamma$  rays, Active interrogation, Fission reactions

*PACS:* 23.20.Lv, 25.85.Ec

---

## 1. Introduction

There has been increased interest in recent years in the nondestructive assay of samples of fissile material for the purpose of quantifying  $^{239}\text{Pu}$  material content [1, 2, 3, 4]. The spectral dependence of  $\beta$ -delayed  $\gamma$  rays emitted from decaying fission products of  $^{235}\text{U}$  and  $^{239}\text{Pu}$  has been established experimentally for time scales on the order of seconds to minutes [5]. Traditionally, a sample of fissile material is interrogated with neutrons or photons and the relative intensities of the  $\beta$ -delayed  $\gamma$ -rays emitted from fission fragments and their decay daughters are used to quantify the fissile material constituents in the sample [6, 7, 8].

Attenuation of the emitted  $\gamma$  rays within the sample and  $\gamma$ -ray detection efficiency will bias the determination of the relative intensities of the  $\beta$ -delayed  $\gamma$ -ray lines unless these effects are known a priori and can be accounted for [9]. The minimization of the range between the energy regions used in forming intensity ratios can reduce, but never fully eliminate, this systematic bias. The method presented here provides an approach independent of intensity ratios via analysis of the temporal response of emitted  $\beta$ -delayed  $\gamma$  radiation from fissile materials. This is accomplished by normalizing the information contained in spectral intensity differences such that only temporal differences remain. The temporal response differences are only affected by the initial population of fission products and associated lifetimes and not by self-attenuation of the sample.

---

\*Corresponding author. Tel.: +1-510-642-5760; fax: +1-510-643-9685.

*Email address:* bethany@nuc.berkeley.edu  
(B. L. Goldblum)

1 An analytical modeling effort was employed  
2 to generate  $\beta$ -delayed  $\gamma$ -ray spectra as a function  
3 of time following pulsed thermal neutron interro-  
4 gation of both pure and mixed samples of  $^{239}\text{Pu}$   
5 and  $^{235}\text{U}$ . Regions of interest in the energy-time  
6 domain were established for identification of the  
7 relative  $^{239}\text{Pu}$  and  $^{235}\text{U}$  content in a mixed sam-  
8 ple. The fraction of the intensity-normalized  $\beta$ -  
9 delayed  $\gamma$ -ray signal over an optimized time in-  
10 terval was sampled using Gaussian statistics to  
11 determine the proportion of  $^{239}\text{Pu}$  in a mixed U-  
12 Pu sample and associated measurement variance.  
13 The basic principles of the temporal  $\beta$ -delayed  $\gamma$ -  
14 ray approach are outlined in Sec. 2, while Sec. 3  
15 provides a description of the model development  
16 and utilization. Within a practical implemen-  
17 tation, long-lived nuclide build-up and Compton  
18 scatter reduces the sensitivity of the technique.  
19 The results for inversion computation with stochas-  
20 tic effects for the ideal, long-lived nuclide build-  
21 up, and Compton scatter cases are provided in  
22 Sec. 4. Concluding remarks are given in Sec. 5.

## 2. Theory

32 Thermal neutron-induced fission of  $^{235}\text{U}$  and  
33  $^{239}\text{Pu}$  produces a well-characterized direct fission  
34 product yield [10]. The chain yield of secondary<sup>1</sup>  
35 fission fragments (i.e., the percent of fissions which,  
36 after prompt neutron emission, result directly in  
37 production of an isotope of mass  $A$ ) resulting from  
38 the thermal fission of  $^{235}\text{U}$  and  $^{239}\text{Pu}$  is illustrated  
39 in Fig. 1. Radioactive decay of the fission frag-  
40 ments produces a decay chain, where the progeny,  
41 if radioactive, build up and/or die away as time  
42 progresses. The difference in the  $\beta$ -delayed  $\gamma$ -  
43 ray intensities arises from the difference in the  
44 independent yields of the fission fragments (i.e.,  
45 the fraction of fissions which, after prompt neu-  
46 tron emission, results directly in that isotope).  
47 Fission fragments comprising the light-mass peak  
48 ( $A \approx 80 - 110$ ) and regions of the heavy-mass  
49 peak ( $A \approx 137 - 144$ ), as shown in Fig. 1, are

57 <sup>1</sup>For simplicity, fission fragments are considered after  
58 prompt neutron emission throughout the remainder of the  
59 text unless otherwise noted.

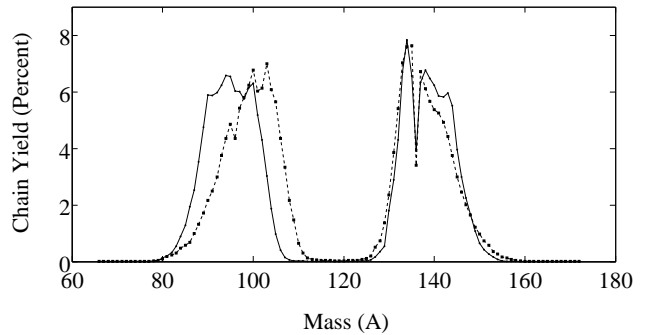


Figure 1: Thermal fission fragment chain yield mass distribution for  $^{235}\text{U}$  (solid line) and  $^{239}\text{Pu}$  (dashed line) [10].

likely to have sufficiently disparate independent yields in the thermal fission of  $^{235}\text{U}$  and  $^{239}\text{Pu}$  such that the spectral dependence of the  $\beta$ -delayed  $\gamma$ -ray signatures from the decay daughters is clearly distinguishable for the two fissile isotopes.

The differences in the independent yields can be observed in both the differences in the intensity and temporal distributions of the  $\gamma$ -ray emission. For a given  $\gamma$ -deexcitation of energy  $E_\gamma$ , the peak region count-rate,  $R$ , may be expressed as the product of the  $\gamma$ -ray emission rate, the detector peak efficiency, and the self-attenuation factor:

$$R(E_\gamma, t) = N(t) * \lambda * I_\gamma * \varepsilon_V(0, E_\gamma) * F_V(\mu, E_\gamma), \quad (1)$$

where  $N(t)$  is the amount of the nuclide at time  $t$ ,  $\lambda$  is the decay constant of the nuclide,  $I_\gamma$  is the  $\gamma$ -ray yield and  $\varepsilon_V(0, E_\gamma)$  is the detector peak efficiency with no self-attenuation of the sample. The self-attenuation factor,  $F_V(\mu, E_\gamma)$  is defined as

$$F_V(\mu, E_\gamma) = \frac{\varepsilon_V(\mu, E_\gamma)}{\varepsilon_V(0, E_\gamma)}, \quad (2)$$

where  $\varepsilon_V(\mu, E_\gamma)$  is the detector peak efficiency given self-attenuation with an average attenuation coefficient,  $\mu$  [11]. In the limit of small sample size,  $F_V(\mu, E)$  will approach unity and differences in the total intensity of peak energy regions can be mapped directly to differences in fission product yields, and thus, to fissile nuclide content. However, if the sample provides appreciable attenuation differences for the  $\gamma$ -rays of interest and this effect is unknown a priori, then a systematic bias is introduced. The magnitude of this

1 systematic error is dependent upon sample com-  
 2 position, geometry and homogeneity, and may be  
 3 reduced by the analysis of  $\gamma$ -rays close in energy  
 4 as to reduce the difference in the self-attenuation  
 5 factors. Peak ratio methods suffer the practical  
 6 limitation of the energy resolution of the detec-  
 7 tor, however, one can utilize temporal differences  
 8 within a single energy region (whose width may  
 9 be defined to be on the order of the energy res-  
 10 olution of the detector) to quantify differences in  
 11 the fissile material content.

12 Differences in the temporal distribution of  $\gamma$ -  
 13 ray emission arise from differences in the indepen-  
 14 dent yields of the nuclides in the decay chain(s)  
 15 that give rise to the nuclide or nuclides that pro-  
 16 duce the dominant  $\gamma$ -ray(s) in the energy bin of  
 17 interest. An example of this phenomenon is given  
 18 at the end of Sec. 3. For the cases in which there  
 19 is only one dominant  $\gamma$ -deexcitation in a given  
 20 energy bin that gives rise to a disparate temporal  
 21 response for  $^{235}\text{U}$  and  $^{239}\text{Pu}$ , the dominant nuclide  
 22 is either produced from different fission fragments  
 23 and/or stems after branching from multiple decay  
 24 chains. In this case, a variation in temporal evolu-  
 25 tion may occur and the observation is essentially  
 26 independent of sample attenuation. When the  
 27 energy range of interest contains dominant  $\gamma$ -ray  
 28 emissions from two or more nuclides, the attenua-  
 29 tion bias is minimized by utilizing  $\gamma$ -ray emissions  
 30 that are closer in energy than the energy resolu-  
 31 tion of the detector. It should be noted that this  
 32 does not reduce attenuation bias to zero, but only  
 33 minimizes it via analysis of  $\gamma$ -ray emissions that  
 34 are close in energy.

### 3. Methodology

35 In order to estimate the temporal response,  
 36 a model was developed to predict the probability  
 37 distribution of  $\beta$ -delayed emission of  $\gamma$ -rays in the  
 38 energy-time domain using a fine binning of 3 keV  
 39 and 50 ms. Each of the energy bins were intensity-  
 40 normalized in order to produce probability dis-  
 41 tributions in time. Although higher-order shape  
 42 components of the response distributions contain  
 43 information, any practical implementation will be  
 44 dominated by the first-order component due to

statistical effects.

Consider the following general case of a linear  
 radioactive decay chain:

$$N_1 \rightarrow N_2 \rightarrow N_3 \rightarrow \dots \rightarrow N_j \rightarrow \dots \rightarrow N_i \rightarrow \dots$$

Initially, an algorithm was employed to determine  
 the isotopes included in a given decay chain. The  
 half-life, decay mode(s), and corresponding branch-  
 ing ratio(s) for the first isotope in the decay chain,  
 $N_1$ , were compiled. A branching ratio thresh-  
 old of 0.01% was applied such that daughter nu-  
 clides with branching ratios of less than 0.01%  
 were omitted from the decay chain, along with  
 their associated  $\gamma$  rays and decay daughters. It is  
 assumed that these nuclides do not significantly  
 contribute to the time-dependent  $\beta$ -delayed  $\gamma$ -ray  
 signal. The daughter isotope,  $N_2$ , was determined  
 by the decay mode(s) of the first isotope in the  
 decay chain,  $N_1$ , and again the associated decay  
 data were compiled. This compilation of decay  
 daughters and associated decay data proceeded  
 iteratively until the nuclide(s) at the end of the  
 chain(s) were stable with respect to radioactive  
 decay. Due to limited decay data, the long-lived  
 isotopes listed in Table 1 were designated as sta-  
 ble. This is reasonable given that the time-scale  
 considered for this analysis is on the order of sec-  
 onds. The decay data, which includes the half-life,  
 decay mode(s), and corresponding branching ra-  
 tio(s), are obtained from the updated nuclear de-  
 cay libraries of the CINDER 2008 actinide trans-  
 mutation code package [12], the Table of Radioac-  
 tive Isotopes (TORI) [13], the Sigma nuclear re-  
 action database [14] and the Evaluated Nuclear  
 Structure Data File (ENSDF-2) [15].

Assuming fission occurs at  $t = 0$ , the amount  
 of any nuclide,  $i$ , in the decay chain,  $N_i$ , present at  
 time  $t$ , was determined by the generalized batch-  
 decay Bateman equation [16]:

$$N_i = \sum_{\ell=1}^{i-1} \left[ N_{\ell}^0 \xi_{\ell} \xi_{\ell+1} \dots \xi_{i-1} \sum_{j=\ell}^i \frac{e^{-\mu_j t}}{\prod_{\substack{k=\ell \\ k \neq j}} (\mu_k - \mu_j)} \right] + N_i^0 e^{-\mu_i t} \quad (3)$$

where the  $\xi$  terms are the partial radioactive de-  
 cay constants, the  $\mu$  terms are the full radioactive

Table 1: Long-lived isotopes designated as stable; The uncertainty given is in the least significant digit(s).

Isotope	Half-life (years)	Uncertainty
$^{70}\text{Zn}$	$> 5 \times 10^{14}$	
$^{82}\text{Se}$	$1.08 \times 10^{20}$	$^{+26}_{-6}$
$^{96}\text{Zr}$	$> 3.8 \times 10^{19}$	
$^{100}\text{Mo}$	$1 \times 10^{19}$	$\pm 10$
$^{128}\text{Te}$	$2.2 \times 10^{24}$	$\pm 3$
$^{130}\text{Te}$	$7.9 \times 10^{20}$	$\pm 10$
$^{136}\text{Xe}$	$> 2.36 \times 10^{21}$	
$^{142}\text{Ce}$	$> 5 \times 10^{16}$	
$^{150}\text{Nd}$	$1.1 \times 10^{19}$	
$^{149}\text{Sm}$	$> 2 \times 10^{15}$	

decay constants, and  $N_\ell^0$  and  $N_i^0$  are the initial amount of the  $\ell$ th and  $i$ th nuclides in the chain, respectively. The partial radioactive decay constant,  $\xi_i$ , for the  $i$ th isotope was calculated by multiplying the full decay constant for the  $i$ th isotope,  $\mu_i$ , by the corresponding normalized branching ratio for decay into the  $(i + 1)$ th isotope, as shown below:

$$\xi_i = \mu_i \frac{\Gamma_{i+1}}{\Gamma_{tot}}, \quad (4)$$

where  $\Gamma_{i+1}$  is the partial width for decay into the  $(i + 1)$ th isotope and  $\Gamma_{tot}$  is the sum of the decay probabilities for all allowed decay modes.

The irradiation period was simulated using a  $\delta$ -pulse of neutrons at  $t = 0$ . For the initial irradiation, fission product independent yields from England and Rider [10] were taken as initial conditions. In the event of a branched radioactive decay chain, the amount of the  $i$ th nuclide in the decay chain at time  $t$ ,  $N_i(t)$ , was obtained by summing the amounts generated from the individual linear chains. If a nuclide was present in the decay chain of multiple fission fragments, the amount of that nuclide was obtained from the sum of the various  $N_i(t)$  values from different decay chains. The counting interval spanned 10 s. The total amount of a given nuclide (in units of atoms per  $10^3$  fissions) at the end of the counting interval was then added to the fission product yields from England and Rider. This sum was utilized as initial conditions in Eq. 3 and thus began the next irradiation and counting cycle.

To generate the time-dependent  $\gamma$ -ray spectra, it was assumed that the amount of any given nuclide at some time  $t^*$  after fission,  $N_i(t^*)$ , is constant over a time bin,  $\Delta t = 50$  ms, and the  $k$ th  $\gamma$ -decay line,  $\Psi_{i,k}(E_\gamma^k, t^*)$ , was then generated for each  $\gamma$  ray from the decay of  $N_i$  using the following equation:

$$\Psi_{i,k}(E_\gamma^k, t^*) = N_i(t^*) * \lambda_i * I_\gamma^k * \Delta t. \quad (5)$$

Here, the  $k$  index designates each individual  $\gamma$ -deexcitation of  $N_i$ ,  $\lambda_i$  is the decay constant of  $N_i$  and  $I_\gamma^k$  is the intensity of the  $k$ th  $\gamma$  ray with energy  $E_\gamma^k$ . A single fission fragment or decay daughter with index  $i$  has  $k_{max}$   $\Psi_{i,k}$  values associated with it (i.e.,  $k_{max}$  is the maximum number of  $\gamma$  rays emitted in the deexcitation of  $N_i$ ). Here, the steady-state approximation is employed (i.e., the amount of the  $i$ th nuclide,  $N_i$ , is assumed to not change significantly over the time bin,  $\Delta t$ ). This is reasonable if the half-lives for the decay processes governing the production and removal of the  $i$ th nuclide are long when compared with the time bin,  $\Delta t$ . The  $\Psi_{i,k}(E_\gamma^k, t^*)$  values were subsequently convolved with a Gaussian function of the form

$$G(E) = \frac{1}{\sigma\sqrt{2\pi}} e^{-\frac{(E-E_\gamma)^2}{2\sigma^2}}, \quad (6)$$

where  $E_\gamma$  represents the centroid of the peak, and

$$\sigma(E_\gamma) = \frac{\sqrt{F\epsilon E_\gamma + W_E^2}}{2.35}. \quad (7)$$

Here,  $F$  is the Fano factor of the detector, assumed to be 0.129 in this case,  $\epsilon$  is 2.96 eV, the average energy required to create an electron-hole pair in germanium, and  $W_E^2$  represents the broadening effects due to electronic noise, approximated as  $(2.07 \text{ keV})^2$  [17].

The effect of the time-dependent Compton continuum was also explored. Two scenarios for  $\gamma$ -ray detection were considered: an idealized case, in which effects of the Compton continuum were neglected, and detection via an ORTEC GEM-10175 coaxial high-purity Germanium (HPGe) detector (dia. = 46.3 mm,  $l = 44.2$  mm) with a relative efficiency of 10% at 1.33 MeV. The low efficiency

1 detector was chosen for modeling a planned ex-  
 2 periment; Though not required, high efficiency  
 3 HPGe detectors are greatly preferred for the mea-  
 4 surements discussed here. For the latter scenario,  
 5 Monte Carlo simulations [18] were employed to  
 6 determine the area of the Compton continuum,  
 7 as well as photopeak, single- and double-escape  
 8 peak efficiencies, in intervals of 100 keV. The area  
 9 of the Compton-continuum and peak detection ef-  
 10 ficiencies were fit with six-order polynomials over  
 11 an energy range of 1 – 7 MeV and interpolation  
 12 was accomplished for each  $\Psi_{i,k}$   $\gamma$ -deexcitation of  
 13  $N_i$ . The Compton-continuum was incorporated  
 14 into the spectra using a constant-intensity shelf-  
 15 model terminating at the Compton edge.

16 Possible sources of error in the time-dependent  
 17  $\beta$ -delayed  $\gamma$ -ray spectra generated with this model  
 18 include:  
 19

- 20 (i) treatment of the neutron irradiation period  
 21 as a  $\delta$ -pulse in time. In a practical experi-  
 22 mental scenario, neutron irradiation will con-  
 23 tinue for a fixed time period and fission frag-  
 24 ments will be generated over the entire irra-  
 25 diation period. However, if the irradiation  
 26 period is short with respect to the time con-  
 27 stants for decay and growth of the isotopes  
 28 of interest, it is reasonable to neglect con-  
 29 tinuous production of fission fragments over  
 30 the irradiation period.
- 31 (ii) modeling of the Compton-continuum shape  
 32 as a shelf that terminates at the Compton  
 33 edge. Although single- and double-escape  
 34 peaks were included in the model, structure  
 35 may be present in the Compton-continuum,  
 36 particularly in the energy range near these  
 37 escape peaks. Omission of the detailed struc-  
 38 ture of the Compton-continuum is not ex-  
 39 pected to affect the overall conclusions pre-  
 40 sented here.
- 41 (iii) incomplete or inaccurate fission product in-  
 42 dependent yields and/or decay libraries. The  
 43 results of this study are limited by the ac-  
 44 curacy of the available nuclear data.

45 Further, it is important to note that as the num-  
 46 ber of irradiation and counting cycles increases,  
 47 the growth of long-lived nuclides will affect the

quantitative sample assessment based on the tem-  
 48 poral dependence of the  $\beta$ -delayed  $\gamma$ -ray signal.  
 49 To investigate this, we consider the time-dependent  
 50  $\beta$ -delayed  $\gamma$ -ray spectrum generated after a single  
 51 thermal neutron irradiation and compare this to  
 52 the spectrum generated after 1001 irradiation and  
 53 counting cycles, as described in detail in Sec. 4.

54 For pure samples of both  $^{235}\text{U}$  and  $^{239}\text{Pu}$ ,  $\beta$ -  
 55 delayed  $\gamma$ -ray spectra were generated after a sin-  
 56 gle irradiation and counting cycle, denoted  $N^{25}(t)$   
 57 and  $N^{49}(t)$ , respectively. For each 3 keV  $\gamma$ -ray en-  
 58 ergy bin, the pure  $^{235}\text{U}$  and  $^{239}\text{Pu}$   $\beta$ -delayed  $\gamma$ -ray  
 59 signals were normalized as a function of time over  
 60 the entire counting interval, denoted  $N_{norm}^{25}(t)$  and  
 61  $N_{norm}^{49}(t)$ , respectively. The fraction of the nor-  
 62 malized response over a time interval from 0 to  
 63  $t_x$  s, where  $t_x \leq 10$  s, was obtained for both pure  
 64  $^{235}\text{U}$  and  $^{239}\text{Pu}$  signals, defined as

$$F^{25} = \int_0^{t_x} N_{norm}^{25}(t) dt \quad (8)$$

and

$$F^{49} = \int_0^{t_x} N_{norm}^{49}(t) dt, \quad (9)$$

65 respectively. The  $t_x$  parameter was determined  
 66 dynamically for each 3 keV energy bin by opti-  
 67 mizing the figure-of-merit (FOM) associated with  
 68 the signal, defined as

$$\text{FOM}(E_\gamma) = \frac{|F^{25} - F^{49}|}{\sqrt{F^{25} + F^{49}}} \sqrt{T^{25} + T^{49}}. \quad (10)$$

69 The first factor in the product on the right-hand-  
 70 side of the equation represents the signal-to-noise  
 71 in the assessment, where the numerator (signal)  
 72 is the difference in the fraction of counts for pure  
 73  $^{235}\text{U}$  and  $^{239}\text{Pu}$  obtained in the time interval from  
 74 0 s up to  $t_x$  s and the denominator (noise) is ob-  
 75 tained using traditional counting statistics. The  
 76 second multiplicand in the product is a statistical  
 77 factor used to scale the signal-to-noise based upon  
 78 the intensity of the non-normalized responses, where

$$T^{25} = \int_0^{t_x} N^{25}(t) dt \quad (11)$$

and

$$T^{49} = \int_0^{t_x} N^{49}(t) dt. \quad (12)$$

Table 2: The top-ten energy bins, listed by bin centroid, with the highest FOM. The energy bin width is 3 keV.

Energy Bin Centroid (keV)			
Single Neutron Pulse		1001 Neutron Pulses	
Idealized	Compton	Idealized	Compton
1217.5	1217.5	1217.5	1217.5
2240.5	1256.5	1259.5	1904.5
1256.5	1259.5	1265.5	1259.5
2435.5	2441.5	1907.5	1220.5
2942.5	1589.5	1220.5	1256.5
2438.5	2240.5	1592.5	1907.5
2441.5	2942.5	1514.5	1091.5
1142.5	1043.5	2435.5	1103.5
2939.5	1169.5	2438.5	1043.5
1760.5	1583.5	1904.5	1088.5

It is important to note that the  $t_x$  determination and FOM ranking is based upon assessment of a sample with no a priori knowledge of the fractional  $^{239}\text{Pu}$  content. That is, the FOM assumes a linear scaling of the normalized fraction of the  $\beta$ -delayed  $\gamma$ -ray response as a function of  $^{239}\text{Pu}$  content in the sample. This is further discussed in Sec. 4.1.

For both a single neutron irradiation and after 1001 neutron pulses, the energy of the top-ten-ranked energy bins for the idealized and Compton-included scenarios are given in Table 2. The  $\beta$ -delayed  $\gamma$ -ray signals in the top-ranked energy bin of  $1217.5 \pm 1.5$  keV, following a single neutron irradiation for pure samples of  $^{235}\text{U}$  and  $^{239}\text{Pu}$ , are illustrated by the bold solid lines in Figs. 2(a) and 2(b), respectively. The strongest contributing fission products to the total spectral intensity are  $^{92}\text{Kr}$  (thin solid line,  $t_{1/2} = 1.85$  s) and  $^{137}\text{I}$  (dotted line,  $t_{1/2} = 24.5$  s). The latter comprises more than 10% of the total signal in the temporal region extending from 0 to  $t_x$  seconds for the  $^{239}\text{Pu}$  response only, but is present in the  $^{235}\text{U}$  response as a non-dominant contributor (dashed line). The contribution from non-dominant nuclides in both Figs. 2(a) and 2(b) is roughly linear over the entire temporal region probed.

The fission fragments responsible for the  $^{92}\text{Kr}$  and  $^{137}\text{I}$  fission products are  $^{92}\text{Se}$ ,  $^{94}\text{Se}$ ,  $^{92}\text{Br}$ ,  $^{93}\text{Br}$ , and  $^{92}\text{Kr}$ , for the  $^{92}\text{Kr}$  isotope, and  $^{137}\text{Sn}$ ,  $^{137}\text{Sb}$ ,

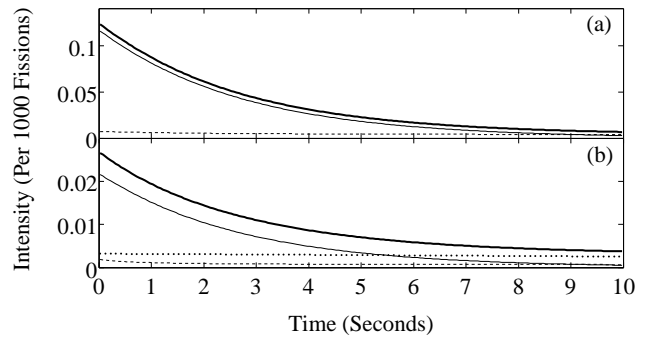


Figure 2: The idealized  $\beta$ -delayed  $\gamma$ -ray response in intensity per  $10^3$  fission events as a function of time, obtained for a pure sample of (a)  $^{235}\text{U}$  and (b)  $^{239}\text{Pu}$ , are represented by the bold solid lines for the top-ranked energy bin of  $1217.5 \pm 1.5$  keV. The solid and dotted lines correspond to the contributions from  $^{92}\text{Kr}$  and  $^{137}\text{I}$ , respectively. The dashed line represents the cumulative contribution of all other nuclides that contribute to the total signal, but comprise less than 10% of the total signal in the temporal region extending from 0 to  $t_x$  seconds, where  $t_x$  is equal to 2.525 s.

$^{138}\text{Sb}$ ,  $^{139}\text{Sb}$ ,  $^{137}\text{Te}$ ,  $^{138}\text{Te}$  and  $^{137}\text{I}$ , for the  $^{137}\text{I}$  isotope, where  $^{92}\text{Kr}$  and  $^{137}\text{I}$  could be formed both directly after fission (after prompt neutron emission) or through the decay of other nuclides. As expected from the thermal fission fragment chain yield mass distribution for  $^{235}\text{U}$  and  $^{239}\text{Pu}$  (See Fig. 1), the corresponding fission fragments have a mass number  $A$  in the range from 92 – 94 and 137 – 139. The difference in  $\beta$ -delayed  $\gamma$ -ray time signatures arises from the disparate fission fragment independent yields of the nuclides in the decay chains (listed above) that give rise to  $^{92}\text{Kr}$  and  $^{137}\text{I}$  (i.e., those isotopes that provide a dominant contribution to the  $\gamma$ -ray spectrum in this energy bin).

## 4. Results

To generate the  $\beta$ -delayed  $\gamma$ -ray spectrum for a mixed sample of  $^{235}\text{U}$  and  $^{239}\text{Pu}$ , the raw, non-normalized  $^{235}\text{U}$  and  $^{239}\text{Pu}$   $\beta$ -delayed  $\gamma$ -ray signals are combined fractionally, as follows:

$$N^{\text{mix}}(t) = \xi[(1 - f)N^{25}(t) + fN^{49}(t)] \quad (13)$$

where  $\xi$  is a factor representing the total number of fission events and  $f$  is the fraction of  $^{239}\text{Pu}$

1 in the sample. Because a specific neutron en-  
 2 ergy spectrum was not assumed, the above treat-  
 3 ment neglects the fission cross sections for  $^{235}\text{U}$   
 4 and  $^{239}\text{Pu}$ . In practice, the  $\beta$ -delayed  $\gamma$ -ray spec-  
 5 tra obtained from the analytical model in units  
 6 of intensity per  $10^3$  fissions must be scaled by the  
 7 energy-dependent fission cross section integrated  
 8 over the relevant neutron energy spectrum. For  
 9 the top-fifty 3 keV energy bins, as determined by  
 10 the FOM ranking, the mixed signal,  $N^{\text{mix}}(t)$  is  
 11 normalized over the 10 s interval and integrated  
 12 over the temporal region up to the  $t_x$  value asso-  
 13 ciated with that energy bin. The signal is defined  
 14 as a Gaussian sampling of the fraction of the nor-  
 15 malized response over a time interval from 0 s up  
 16 to  $t_x$  s. That is,

$$F^{\text{mix}} = \frac{\int_0^{t_x} N^{\text{mix}}(t) dt}{\int_0^{10 \text{ s}} N^{\text{mix}}(t) dt} \quad (14)$$

26 For the top-fifty energy bins, as determined by the  
 27 FOM ranking, with  $\xi = 10^6$ , the normalized frac-  
 28 tion of the  $\beta$ -delayed  $\gamma$ -ray spectrum for a mixture  
 29 of  $^{235}\text{U}$  and  $^{239}\text{Pu}$ , determined over a time inter-  
 30 val from 0 s up to the associated  $t_x$  value, was  
 31 sampled with Gaussian statistics for 10,000 trials.  
 32 That is, a single trial consists of sampling all  
 33 of the top-fifty energy bins once and solving for  
 34 the normalized fraction. A number of identical  
 35 trials were obtained to provide the expected vari-  
 36 ance in the measurement. Based upon the nor-  
 37 malized fraction of the  $\beta$ -delayed  $\gamma$ -ray spectrum,  
 38 an assessment of the  $^{239}\text{Pu}$  fraction in the mixed  
 39 sample, as well as the associated uncertainty, is  
 40 obtained.

#### 4.1. Idealized case for a single $\delta$ -pulse of neutrons

48 The probability for obtaining a given normal-  
 49 ized fraction of the  $\beta$ -delayed  $\gamma$ -ray spectrum in  
 50 the top-ranked  $1217.5 \pm 1.5$  keV energy bin via  
 51 a single neutron irradiation, neglecting Compton  
 52 scattering, was sampled with Gaussian statistics  
 53 for 10,000 trials. The normalized fraction of the  
 54  $\beta$ -delayed  $\gamma$ -ray signal was determined for a 50%  
 55 mixture of  $^{235}\text{U}$  and  $^{239}\text{Pu}$ , integrated over a time  
 56 interval from 0 s up to the  $t_x$  value of 2.525 s. A  
 57 Gaussian fit of the sampled data with a mean,  
 58  
 59  
 60  
 61  
 62  
 63  
 64  
 65

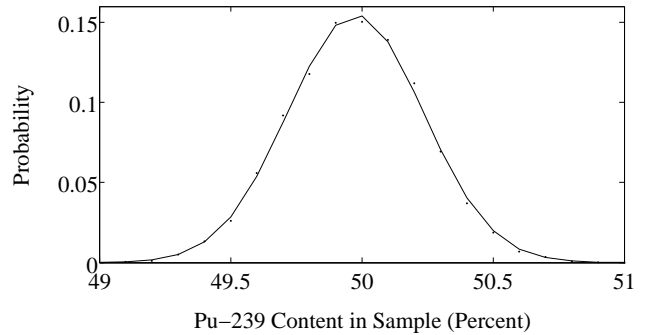


Figure 3: The probability of determining a given  $^{239}\text{Pu}$  sample content, in percent, from spectral data in the top-fifty-ranked energy bins obtained via a single neutron irradiation, neglecting the effects of Compton scattering. The solid line is a Gaussian fit of the data with a mean of 49.98% and a FWHM of 0.61%.

$\bar{x}$ , of 0.568 and a full width at half maximum (FWHM) of 0.001 was obtained. The normalized fraction of the mixed  $\beta$ -delayed  $\gamma$ -ray signal was utilized to determine the percentage of  $^{239}\text{Pu}$  in a mixed sample. This process was repeated for the top-fifty-ranked energy bins and the probability for determining a given  $^{239}\text{Pu}$  fractional sample content, as obtained from the  $\beta$ -delayed  $\gamma$ -ray spectral data via a single neutron irradiation, neglecting the effects of Compton scattering, is illustrated in Fig. 3. The data points represent a sampling with 10,000 trials for a 50% mixture of  $^{235}\text{U}$  and  $^{239}\text{Pu}$ . The solid line is a Gaussian fit of the sampled data with  $\bar{x} = 49.98\%$  and FWHM= 0.61%. This corresponds to a  $^{239}\text{Pu}$  content in the sample of  $49.98 \pm 0.26\%$ , representing excellent agreement with the 50%  $^{239}\text{Pu}$  sample content in the simulated  $\beta$ -delayed  $\gamma$ -ray spectral response for an idealized, single irradiation scenario. The analysis was repeated for a mixed U-Pu sample of 10%  $^{239}\text{Pu}$  and 90%  $^{239}\text{Pu}$  with assessed  $^{239}\text{Pu}$  sample contents of  $9.97 \pm 0.36\%$  and  $89.99 \pm 0.17\%$ , respectively.

Figure 4(a) showcases the variation in the normalized fraction of the mixed  $\beta$ -delayed  $\gamma$ -ray signal as obtained from the temporal signal in the  $1217.5 \pm 1.5$  keV energy bin as a function of the percentage of  $^{239}\text{Pu}$  in a mixed sample. As mentioned above, ranking of the top energy bins for assessment of the temporal and spectral dependence of the  $\beta$ -delayed  $\gamma$ -ray signal via the FOM

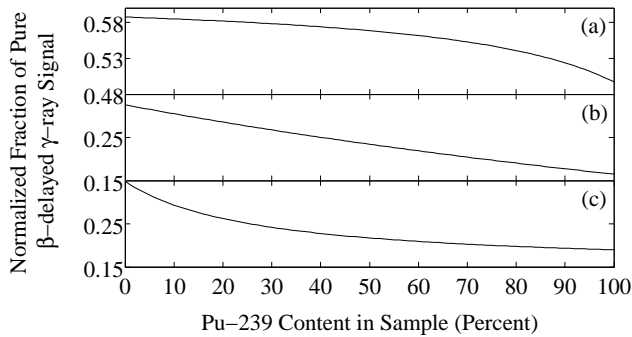


Figure 4: The normalized fraction of the  $\beta$ -delayed  $\gamma$ -ray response obtained from a single pulse, idealized scenario for the (a)  $1217.5 \pm 1.5$  keV, (b)  $2240.5 \pm 1.5$  keV, and (c)  $2699.5 \pm 1.5$  keV energy bins as a function of the percent of  $^{239}\text{Pu}$  in a mixed sample. Note the zero-suppressed ordinate axes.

is based upon the assumption of linear scaling of  $F^{\text{mix}}$  with the fractional  $^{239}\text{Pu}$  sample content. However, as indicated in Fig. 4(a), non-linearities exist in the normalized fraction of the mixed  $\beta$ -delayed  $\gamma$ -ray spectrum as a function of the percentage of  $^{239}\text{Pu}$  in a mixed sample. Here, the curvature of the normalized fraction of the mixed  $\beta$ -delayed  $\gamma$ -ray spectrum as a function of the percentage of  $^{239}\text{Pu}$  is greater for high  $^{239}\text{Pu}$  content. That is, for this energy bin and simulated data, the non-linearities result in a more accurate assessment for high  $^{239}\text{Pu}$  content samples.

Now consider, in contrast, the normalized fraction of the  $\beta$ -delayed  $\gamma$ -ray response obtained from an idealized, single irradiation for the  $2240.5 \pm 1.5$  keV and  $2699.5 \pm 1.5$  keV energy bins as a function of  $^{239}\text{Pu}$  sample content, graphically illustrated in Figs. 4(b) and 4(c), respectively. Figure 4(b) shows a roughly linear relationship between the normalized fraction of the mixed  $\beta$ -delayed  $\gamma$ -ray signal as a function of the percentage of  $^{239}\text{Pu}$  in a mixed sample and thus, should provide reasonable assessment of the fractional  $^{239}\text{Pu}$  content regardless of the sample composition. In contrast, Fig. 4(c) showcases a highly nonlinear relationship between the normalized fraction of the mixed  $\beta$ -delayed  $\gamma$ -ray signal and the percentage of  $^{239}\text{Pu}$  in a mixed sample, which would be more appropriate for assessment of low  $^{239}\text{Pu}$  content samples. Given the possible non-linearities in the normalized fraction of the mixed

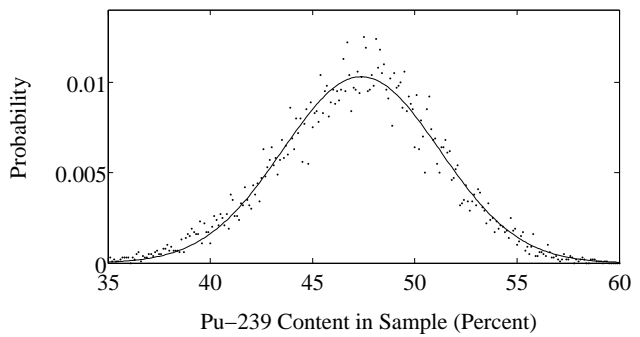


Figure 5: The probability of determining a given  $^{239}\text{Pu}$  sample content, in percent, obtained from a single neutron irradiation, with Compton effects included, obtained from the FOM-derived top-fifty-ranked energy bins. The solid line is a Gaussian fit of the data with a mean of 47.38% and FWHM of 9.02%.

$\beta$ -delayed  $\gamma$ -ray signal as a function of the percentage of  $^{239}\text{Pu}$  in a mixed sample, an iterative approach is suggested in which the value of the  $^{239}\text{Pu}$  fraction in the mixed sample obtained from the first iteration is used to determine newly optimized values of  $t_x$  values and ranking of energy bins. The assessment is repeated until the derived percentage of  $^{239}\text{Pu}$  in the mixed sample converges.

#### 4.2. Effects of the Compton-continuum

The probability for determining a given  $^{239}\text{Pu}$  fractional sample content, as obtained from the  $\beta$ -delayed  $\gamma$ -ray spectral data in the top-fifty-ranked energy bins via a single neutron irradiation, and including the effects Compton scattering, is illustrated in Fig. 5. The data points represent a sampling with 10,000 trials for a 50% mixture of  $^{235}\text{U}$  and  $^{239}\text{Pu}$ . The solid line is a Gaussian fit of the data with  $\bar{x} = 47.38\%$  and  $\text{FWHM} = 9.02\%$  and thus, we derive a fractional  $^{239}\text{Pu}$  content in the sample of  $47.38 \pm 3.84\%$ .

The increased uncertainty in this assessment relative to the ideal scenario is due, in part, to the decreased intensity of the non-normalized, time-dependent,  $\beta$ -delayed  $\gamma$ -ray responses. For the top ranked energy bin of 1216-1219 keV and pure samples of both  $^{235}\text{U}$  and  $^{239}\text{Pu}$  after a single neutron irradiation, shown in Figs. 6(a) and Figs. 6(b), respectively, a decreased total  $\beta$ -delayed  $\gamma$ -ray intensity (solid bold line) is observed. Here, the

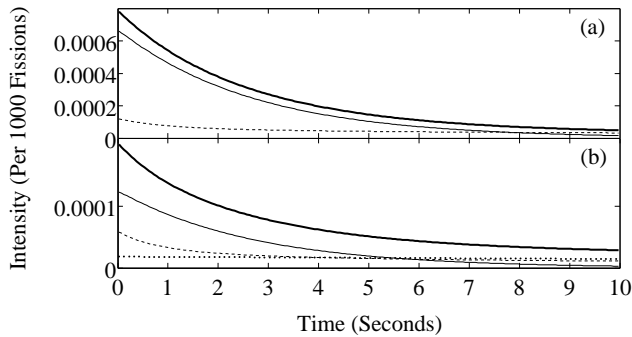


Figure 6: The  $\beta$ -delayed  $\gamma$ -ray responses, including the effects of Compton scattering, in intensity per  $10^3$  fission events as a function of time, obtained for a pure samples of (a)  $^{235}\text{U}$  and (b)  $^{239}\text{Pu}$  after a single neutron irradiation, are represented by the bold solid lines. The solid and dotted lines correspond to the contributions from  $^{92}\text{Kr}$  and  $^{137}\text{I}$ , respectively. The dashed line represents the cumulative contribution of all other nuclides that contribute to the total signal, but comprise less than 10% of the total signal in the temporal region extending from 0 to  $t_x$  seconds.

strongest contributing fission products to the total spectral intensity are again  $^{92}\text{Kr}$  (thin solid line) and  $^{137}\text{I}$  (dotted line). However, the relative contribution of non-dominant nuclides (i.e., those nuclides that contribute to the signal, but comprise less than 10% of the total signal in the temporal region extending from 0 to  $t_x$  seconds, where  $t_x$  is equal to 2.675 s) is increased compared to the idealized, single neutron irradiation scenario illustrated in Fig. 2. For a single neutron irradiation, the number of nuclides present as non-dominant contributors in the idealized scenario is 187, compared to 216 non-dominant nuclides for the Compton-included scenario. Although the uncertainty in the assessment is larger due to the time-dependence of the Compton continuum, we still obtain agreement within one standard deviation with the simulated  $^{239}\text{Pu}$  sample content of 50%. Nonetheless, the data suggest that Compton-suppression of the  $\beta$ -delayed  $\gamma$ -ray signals will result in a quantitative assessment of the  $^{239}\text{Pu}$  sample content with decreased uncertainty. This could be accomplished, for example, by utilizing an annular bismuth germanate shield mounted at the rear face of the germanium crystal.

### 4.3. Effects of longer-lived nuclides

An assessment of the  $^{239}\text{Pu}$  fractional sample content was repeated for both the idealized and Compton-included scenarios after 1001 neutron pulses (corresponding to approximately 2.8 h). Using the top-fifty-ranked energy bins, the normalized fraction of the mixed  $\beta$ -delayed  $\gamma$ -ray signal, obtained after 1001 irradiation and counting cycles, was utilized to determine the percentage of  $^{239}\text{Pu}$  in a mixed sample. The probability distribution for assessing a given  $^{239}\text{Pu}$  fractional sample content, neglecting the effects of Compton scattering, was obtained using a sampling of 10,000 trials for a 50% mixture of  $^{235}\text{U}$  and  $^{239}\text{Pu}$ . A Gaussian fit of the sampled data was obtained with  $\bar{x} = 50.00\%$  and  $\text{FWHM} = 0.38\%$ . The assessed  $^{239}\text{Pu}$  content in the sample of  $50.00 \pm 0.16\%$  again represents excellent agreement with the simulated 50%  $^{239}\text{Pu}$  sample content.

The effects of Compton scattering on the assessment of the  $^{239}\text{Pu}$  fractional sample content was investigated following 1001 neutron irradiation and counting cycles. Using a sampling of 10,000 trials for a 50% mixture of  $^{235}\text{U}$  and  $^{239}\text{Pu}$ , a Gaussian fit of the data was obtained with  $\bar{x} = 48.98\%$  and  $\text{FWHM} = 5.99\%$ . The derived fractional  $^{239}\text{Pu}$  sample content of  $48.98 \pm 2.54\%$  provides an accurate assessment of the simulated  $^{239}\text{Pu}$  sample content of 50%. The decreased uncertainty in the assessment, relative to the Compton-included, single neutron irradiation scenario, is primarily due to improved statistics (i.e., increased intensity of the  $\beta$ -delayed  $\gamma$ -ray signal).

To explore the effect of the growth of longer-lived nuclides on the temporal dependence of the  $\beta$ -delayed  $\gamma$ -ray signal, the strongest contributing nuclides to the top ranked energy bin of 1216-1219 keV were determined for a Compton-included scenario after 1001 neutron pulses. This is illustrated graphically in Fig. 7 for pure samples of both (a)  $^{235}\text{U}$  and (b)  $^{239}\text{Pu}$ . The bold solid line represents the total signal and the solid and dotted lines correspond to the contributions from  $^{92}\text{Kr}$  and  $^{137}\text{I}$ , respectively. In contrast to the  $\beta$ -delayed  $\gamma$ -ray signal from pure  $^{235}\text{U}$  after a single neutron irradiation, the  $^{137}\text{I}$  represents a domi-

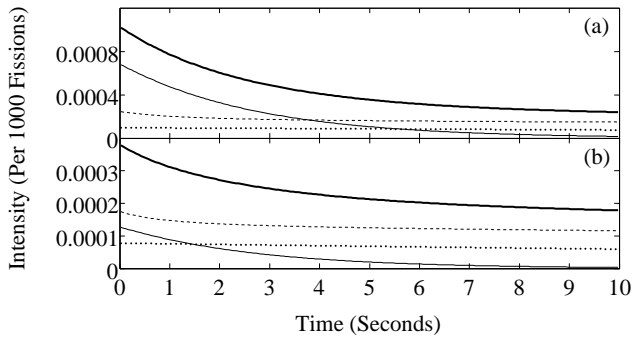


Figure 7: The  $\beta$ -delayed  $\gamma$ -ray responses in intensity per  $10^3$  fission events as a function of time, with the effects of Compton scattering included, obtained for a pure samples of (a)  $^{235}\text{U}$  and (b)  $^{239}\text{Pu}$  after 1001 neutron pulses, are represented by the bold solid lines. The solid and dotted lines correspond to the contributions from  $^{92}\text{Kr}$  and  $^{137}\text{I}$ , respectively. The dashed line represents the cumulative contribution of all other nuclides that contribute to the total signal, but comprise less than 10% of the total signal in the temporal region extending from 0 to  $t_x$  seconds, where  $t_x$  is equal to 2.275 s.

nant contribution after 1001 neutron pulses. However, the contribution is roughly linear with time and thus, does not significantly contribute to the quantitative assessment. The dashed line represents the cumulative contribution of all other nuclides that contribute to the total signal, but comprise less than 10% of the total signal in the temporal region extending from 0 to  $t_x$  seconds. The contribution of longer-lived nuclides is non-linear at short time scales and more prominent after extended neutron irradiation and counting cycles (compare Fig. 7 with Figs. 2 and 6). The temporal dependence of the signal remains dominated by the contribution from  $^{92}\text{Kr}$ . It is the difference in the temporal dependence of the  $\beta$ -delayed  $\gamma$ -ray signals from  $^{235}\text{U}$  and  $^{239}\text{Pu}$  that gives rise to the quantitative assessment and this difference, arising from the disparate fission fragment independent yields, is preserved.

## 5. Conclusions

The temporal dependence of the intensity of the delayed  $\gamma$  ray signal in different energy bins provides novel isotopic-dependent signatures for the quantitative assay of  $^{239}\text{Pu}$  and  $^{235}\text{U}$  content in a mixed sample. However, the time-dependent ef-

fects of the Compton continuum serve to increase the uncertainty in the assay of the fractional  $^{239}\text{Pu}$  sample content. Given that the relative intensities of  $\beta$ -delayed  $\gamma$ -rays of different energies are not used for the determination of the fractional  $^{239}\text{Pu}$  sample content, effects due to variation of detector efficiency or attenuation of the emitted  $\gamma$  rays in the sample are minimized, effectively removing what was formerly one of the largest sources of systematic uncertainty in the conventional quantitative assay of complex samples (e.g., inhomogeneous samples containing multiple fissile nuclides [19]) using photon interrogation. In addition, it is not required that  $\gamma$ -decay lines are unobscured by other peaks, because the cumulative temporal response is comprised of the  $\beta$ -delayed  $\gamma$ -ray signals emitted from several fission fragments and their decay daughters. Provided  $\gamma$  rays are sufficiently penetrating to readily escape the sample, this innovative methodology can be applied to samples containing other fissionable isotopes. This means of analysis represents a first-order correction to the traditional spectral analysis of  $\beta$ -delayed  $\gamma$ -ray signatures and provides a potential pathway to the quantitative assay of  $^{239}\text{Pu}$  content in spent fuel and for quantitative nuclear forensic applications. However, empirical validation of this methodology and experimental feasibility of the method using both pure and mixed samples of U-Pu must first be demonstrated.

## Acknowledgments

We wish to thank S.G. Prussin for fruitful discussions and advice. We gratefully acknowledge the contributions of R.D. Crabbs and J. Lorenzo. This work was supported, in part, by the University of California, Berkeley, Chancellor's Postdoctoral Fellowship Program, the Clare Boothe Luce Foundation, the Berkeley Nuclear Research Center (00F8F4 University of California Lab Fees Research Program, Award Number 09-LR-01-117616-VUJJ), the Next Generation Safeguard Initiative of the Office of Nonproliferation and International Security (US DOE, NA-241), the MPACT campaign of the FCR&D program of the Office of Nuclear Energy (US DOE), and the Director, Of-

1 fice of Science of the US Department of Energy  
2 at Lawrence Berkeley National Laboratory under  
3 contract number DE-AC02-05CHI1231.  
4

## 6 References

- 8 [1] S.J. Tobin, S.F. Demuth, M.L. Fensin, J.S. Hendricks,  
9 H.O. Menlove, M.T. Swinhoe, "Determination of Plu-  
10 tonium Content in Spent Fuel with NDA - Why an  
11 Integrated Approach?" Annual Meeting of the Insti-  
12 tute of Nuclear Material Management, Nashville, TN,  
13 July 2008 (LA-UR-08-03763).
- 14 [2] M.L. Felsin, S.J. Tobin, N.P. Sandoval, M.T. Swin-  
15 hoe and H.O. Menlove, "A Monte Carlo Based Spent  
16 Fuel Analysis Safeguards Strategy Assessment," Los  
17 Alamos National Laboratory Report No. LA-UR-09-  
18 01632, 2009.
- 19 [3] A. Gavron, L.E. Smith, J.J. Ressler, "Analysis of  
20 spent fuel assemblies using a lead slowing down spec-  
21 trometer," Nucl. Instrum. Meth. A 602 (2009) 581-  
22 587.
- 23 [4] B.J. Quiter, B.A. Ludewigt, V.V. Mozin, and  
24 S.G. Prussin, "Nuclear Resonance Fluorescence for  
25 Materials Assay," IEEE Transactions on Nuclear Sci-  
26 ence (accepted for publication).
- 27 [5] E.B. Norman, S.G. Prussin, R.-M. Larimer, H.  
28 Shugart, E. Browne, A.R. Smith, R.J. McDonald, H.  
29 Nitsche, P. Gupta, M.I. Frank, T.B. Gosnell, "Signa-  
30 tures of fissile materials: high-energy  $\gamma$  rays following  
31 fission," Nucl. Instrum. Meth. A 521 (2004) 608-610.
- 32 [6] M. Gmar and J.M. Capdevila, "Use of delayed  
33 gamma spectra for detection of actinides (U,Pu) by  
34 photofission," Nucl. Instrum. Meth. 422 (1999) 841-  
35 845.
- 36 [7] R.E. Marrs, E.B. Norman, J.T. Burke, R.A. Macri,  
37 H.A. Shugart, E. Browne, A.R. Smith, "Fission-  
38 product gamma-ray line pairs sensitive fo fissile ma-  
39 terial and neutron energy," Nucl. Instrum. Meth. A  
40 592 (2009) 463-471.
- 41 [8] F. Carrel, M. Agelou, M. Gmar, F. Lainé, J. Lorida,  
42 J.-L. Ma, C. Passard, and B. Poumaréde, "Identi-  
43 fication and Differentiation of Actinides Inside Nu-  
44 clear Waste Packages by Measurement of Delayed  
45 Gammas," IEEE Transactions on Nuclear Science 57  
46 (2010) 2862-2871.
- 47 [9] D.H. Beddingfield, F.E.Cecil, "Identification of fissile  
48 materials from fission product gamma-ray spectra,"  
49 Nucl. Instrum. Meth. A. 417, 405 (1998).
- 50 [10] T.R. England, B.F. Rider, Evaluation and Compi-  
51 lation of Fission Product Yields, Los Alamos Na-  
52 tional Laboratory Report LA-UR-94-3106, ENDF-  
53 349, 1994.
- 54 [11] M. Korun, "Self-Attenuation Factors in Gamma-Ray  
55 Spectrometry," Czechoslovak Journal of Physics 49,  
56 (1999) 429-434.
- 57 [12] W.B. Wilson, S.T. Cowell, T.R. England, A.C. Hayes  
58 and P. Moller, "A Manual for CINDER'90 Version  
59 07.4 Codes and Data," LA-UR-07-9412 (December  
60 2007, Version 07.4.2 updated March 2008).
- 61 [13] *Table of Isotopes*, 8th ed., edited by R.B. Firestone  
62 and V. S. Shirley (Wiley, New York, 1996), Vol. II.
- 63 [14] B. Pritychenko and A.A. Sonzogni, Nucl. Data Sheets  
64 109, 2822 (2008).
- 65 [15] Evaluated Nuclear Structure Data File (6/21/2006),  
a computer file of evaluated experimental nuclear  
structure data maintained by the National Nuclear  
Data Center, Brookhaven National Laboratory.
- [16] M. Benedict, T.H. Pigford and H.W. Levi, *Nuclear  
Chemical Engineering*, 2nd Ed. (McGraw-Hill, 1981),  
Ch. 2.
- [17] G.F. Knoll, *Radiation Detection and Measurement*,  
3rd Ed. (John Wiley & Sons, 2000), Ch. 4.
- [18] D. B. Pelowitz, ed., "MCNPX User's Manual, Version  
2.6.0," LA-CP-07-1473 (April 2008); J. S. Hendricks  
et al., "MCNPX 2.6.0 Extensions," LA-UR-08-2216  
(April 2008).
- [19] M.L. Fensin, S.J. Tobin, M.T. Swinhoe, H.O. Menlove  
and N.P. Sandoval, "A Monte Carlo Based Spent Fuel  
Analysis Safeguards Strategy Assessment," LA-UR-  
09-01632 (September 2009).